Perioperative Precision Medicine

Zentime

RESEARCH ARTICLE

Therapeutic potential of Dunhuang Mofeng ointment in rheumatoid arthritis: Integrative network pharmacology and experimental validation

Haolong Zhang[1,2,*], Jing Pan[1,*], Zhijing Song[1]

[1]Clinical College of Traditional Chinese Medicine, Gansu University of Chinese Medicine, Lanzhou 730000, Gansu, China.
[2]The First Affiliated Hospital of Henan Medical University, Xinxiang 453100, Henan, China.
[*]The authors are co-first authors.

Corresponding author: Zhijing Song.

Address correspondence to: Zhijing Song, Clinical College of Traditional Chinese Medicine, Gansu University of Chinese Medicine, No. 35 Dingxi East Road, Chengguan District, Lanzhou 730000, Gansu, China.
E-mail: songzhijing2020@163.com.

Received November 11, 2025; Accepted March 16, 2026; Published March 31, 2026

DOI: 10.61189/372252akozze

Abstract

Objective: This study integrated network pharmacology and molecular docking to identify the active constituents, core targets, and potential mechanisms of Dunhuang Mofeng ointment in treating rheumatoid arthritis (RA). The therapeutic efficacy was validated using a collagen-induced arthritis (CIA) rat model. **Methods:** Bioactive compounds and target molecules of Dunhuang Mofeng ointment were identified using R language-based network pharmacological analysis. These were integrated with RA-related differential genes from the GEO database to construct regulatory and protein-protein interaction networks. Gene ontology and Kyoto Encyclopedia of Genes and Genomes enrichment analyses were performed to elucidate intervention mechanisms. Molecular docking simulations validated the conformational stability of core targets. A seven-week CIA rat model was established to assess therapeutic effects, including general health, joint swelling, limb deformities, serum inflammatory markers, and mRNA expression of key targets in joint tissues, thereby validating the network pharmacology predictions. **Results:** The core active ingredients were quercetin, apigenin, luteolin, aloe-emodin, and emodin. Primary therapeutic targets included STAT1, CDK4, CCND1, MCL1, FOS, CDKN1A, and MYC, with anti-inflammatory effects mediated through pathways such as JAK-STAT, PI3K-Akt, and Toll-like receptor pathways. After 7 weeks of treatment, CIA rats showed significant improvements, including reduced joint swelling and deformity, decreased pro-inflammatory cytokines, and increased anti-inflammatory cytokine IL-10. mRNA expression of STAT1, CDK4, CCND1, MCL1, FOS, and MYC in joint tissues was significantly downregulated ($P<0.05$), while CDKN1A expression was upregulated ($P<0.001$). The medium-dose and Western medicine groups exhibited pronounced therapeutic effects. **Conclusion:** Dunhuang Mofeng ointment may exert therapeutic effects in RA by modulating pro-inflammatory cytokines and regulating key genes. These findings support its potential as an effective intervention for RA.

Keywords: Dunhuang Mofeng ointment, Rheumatoid arthritis, Network pharmacology, Molecular docking, Experimental verification

1 INTRODUCTION

Rheumatoid arthritis (RA) is a systemic autoimmune disorder marked by chronic synovitis and progressive joint destruction. While primarily characterized by destructive inflammatory synovitis, RA frequently manifests with systemic complications, including skeletal involvement, cardiovascular dysfunction, metabolic disturbances, and cognitive impairments [1, 2].

Epidemiological data estimate the global annual incidence of RA at approximately 3 cases per 10,000 individuals, with a prevalence approaching 1% [3]. Although the precise etiology of RA remains elusive, existing research highlights the pivotal roles of genetic predisposition and environmental factors in disease onset and progression [4]. Current therapeutic strategies aim to mitigate inflammatory responses, alleviate clinical symptoms, and decelerate disease progression. Disease-modifying anti-rheumatic drugs (DMARDs) represent the cornerstone of RA management, effectively suppressing the inflammatory cascade and preventing further joint structural damage; however, their efficacy and safety profiles warrant further refinement [5].

DMARDs, primarily biologics based on monoclonal antibodies or receptor constructs, target cytokines, cytokine receptors, or cell surface antigens to exert their therapeutic effects. These agents function by inhibiting ligand-receptor interactions, depleting specific cell populations, or disrupting cell-cell communication. However, as protein-based therapeutics requiring intravenous or subcutaneous administration, these DMARDs are inherently limited to extracellular or cell-surface mechanisms, precluding direct modulation of intracellular signaling pathways. This represents a critical constraint in addressing certain intracellular pathological mechanisms [6]. While DMARDs have demonstrated remarkable efficacy in suppressing autoimmune responses and slowing disease progression, their immunosuppressive properties heighten the risk of infections, particularly respiratory and opportunistic infections, especially in immunocompromised patients. Concurrently, the use of oral non-steroidal anti-inflammatory drugs is often restricted by significant dose-dependent adverse effects, including cardiovascular, renal, and hematological toxicities. As a highly heterogeneous condition, RA continues to present significant unmet therapeutic needs, including suboptimal responses to existing treatments, failure to achieve immune homeostasis or complete remission, and the inability to repair damaged tissues. Addressing these challenges requires a more comprehensive understanding of the disease's pathogenesis to overcome its complexity and heterogeneity. Interestingly, treatment preferences among Chinese RA patients reveal a diversified approach. A study involving 18 patients found that 7 utilized DMARDs, 6 transitioned to traditional Chinese medicine (TCM) after discontinuing conventional treatments, and 5 combined DMARDs with TCM therapies [7]. These findings suggest that TCM may offer unique benefits in RA management, not only by alleviating symptoms but also by providing a potential alternative or complementary therapeutic strategy.

The formulation of Dunhuang Mofeng ointment originates from the Dunhuang manuscript *The Second Kind of the Dead Ming's Pulse Classics*. The original recipe, known as the Mofeng Ointment Formula, is preserved in the National Library of France under the catalog number P·3287. The extant fragments of the *Pulse Classics* contain 13 ancient prescriptions, of which 7 are described in detail, with Mofeng Ointment being one of the more thoroughly documented. This historical recipe is not only comprehensive in its composition but also includes meticulous instructions for its preparation and application. The Mofeng Ointment formula consists of seven medicinal herbs, including *Aconitum carmichaelii*, *Salvia miltiorrhiza*, *Zanthoxylum bungeanum*, *Ligusticum chuanxiong*, *Rheum palmatum*, *Croton tiglium*, and *Angelica sinensis*, providing a rich clinical background for its use. As a topical formulation, Mofeng Ointment exerts its therapeutic effects locally by permeating the skin to target the affected area, thereby minimizing systemic absorption and reducing the risk of systemic side effects, particularly those associated with immunosuppression, such as infection. In a similar vein, Voltaren ointment (diclofenac diethylamine cream), also applied topically, is associated with a low incidence of systemic reactions. As a potent inhibitor of prostaglandin synthesis, Voltaren is known for its significant anti-inflammatory and analgesic effects. When applied locally, its active ingredients penetrate the skin to reach the site of inflammation, alleviating both acute and chronic inflammatory responses, particularly those induced by trauma or rheumatism, and providing marked reductions in swelling and pain [8-10]. Given its extensive clinical use, Voltaren ointment was chosen as the treatment control group for the comparative analysis in this study.

In this study, leveraging computer-aided drug design technology and considering the multi-component, multi-target, and multi-pathway characteristics of Dunhuang Mofeng ointment, we systematically explored its potential active ingredients, molecular targets, and associated signaling pathways. The aim was to elucidate the underlying mechanisms through which the ointment intervenes in the pathogenesis of RA. Concurrently, the therapeutic efficacy of Dunhuang Mofeng ointment in RA was validated through animal experiments, with Voltaren ointment serving as the control treatment group for comparative analysis. This study provides a comprehensive investigation of the intervention mechanisms of Dunhuang Mofeng ointment on RA from multiple dimensions, thereby offering a theoretical foundation for its clinical application. Additionally, it presents novel insights and perspectives for advancing the research and development of TCM as an external therapeutic modality. The technical framework of the study is illustrated in **Figure 1**.

2 MATERIALS AND METHODS

2.1 Experimental animal

In this study, 60 specific pathogen-free (SPF)-grade Sprague-Dawley rats (190±10 g, evenly distributed by sex) were procured from SPF (Beijing) Biotechnology Co., Ltd. (License No. SCXK (Beijing) 2019-0010). Ethical approval was granted by Gansu University of Chinese Medicine (SY2023-966). The animals were housed in the SPF-certified animal facility at the Research and Experiment Center of Gansu University of

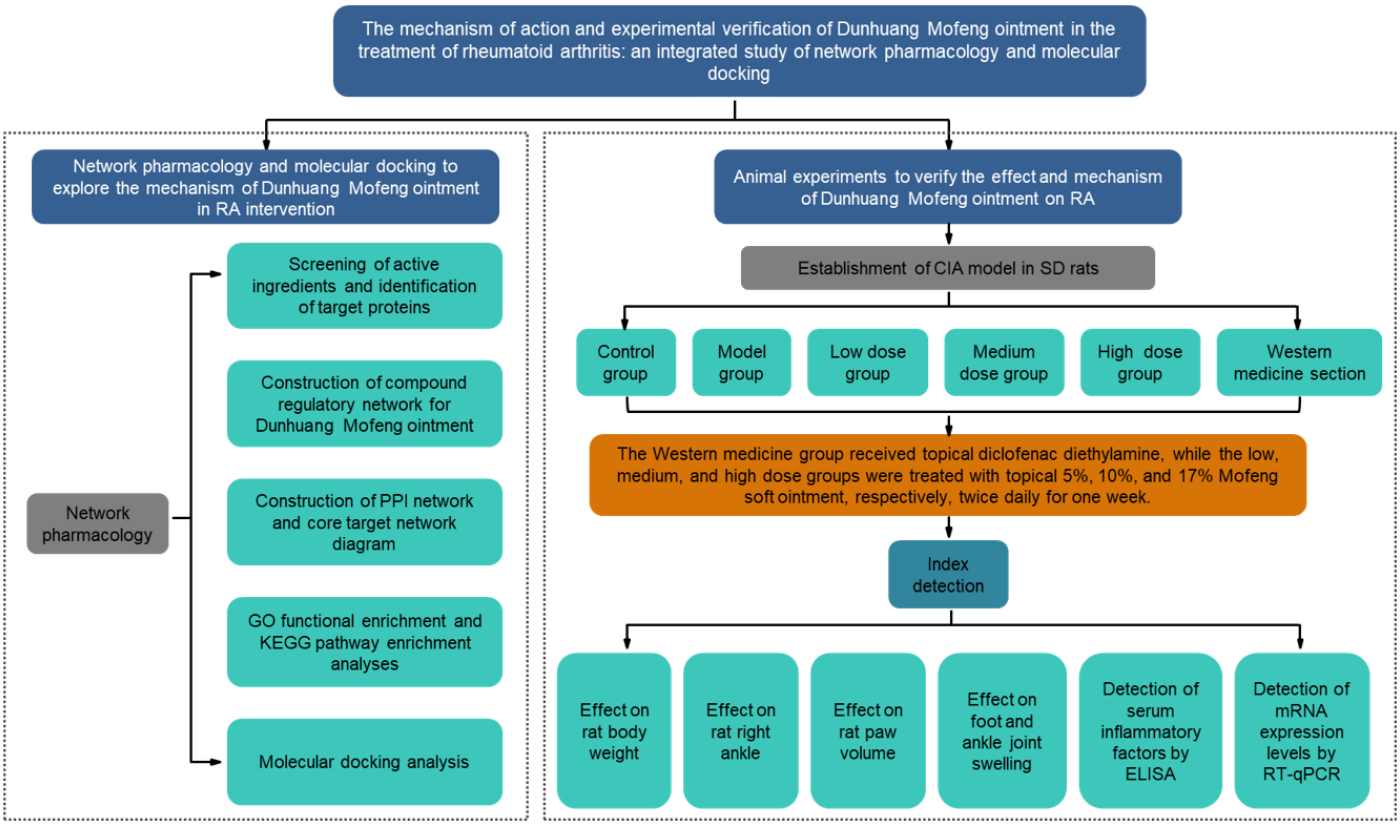

Figure 1. The technical framework of this study. PPI, protein-protein interaction; GO, Gene Ontology; KEGG, Kyoto Encyclopedia of Genes and Genomes; ELISA, Enzyme-Linked Immunosorbent Assay; RT-qPCR, Real-Time Quantitative Polymerase Chain Reaction.

Chinese Medicine under strictly controlled environmental conditions. Temperature was maintained at 23-24 °C, relative humidity at 45-65%, and a 12-hour light/dark cycle was implemented. Throughout the experiment, the rats had ad libitum access to food and water. Following a one-week acclimatization period, the experimental protocol was formally initiated.

2.2 Experimental drugs and reagents

The Dunhuang Mofeng ointment (DHMF2023) used in this study was independently developed by Gansu University of Traditional Chinese Medicine and prepared at concentrations of 5%, 10%, and 17%. These concentrations were selected based on preliminary experimental observations and the commonly used concentration ranges reported in previous studies of topical TCM preparations. Three dose gradients (low, medium, and high) were established to evaluate the potential dose–response relationship of the ointment in the rat model. The control drug, diclofenac diethylamine emulsion (Voltaren), was supplied by GSK Consumer Healthcare SARL (Batch No. EC8P). Key experimental materials included bovine type II collagen (Chondrex, USA; Catalog No. 220241) and complete Freund's adjuvant (CFA) (Sigma, USA; Lot No. SLBR1681V). Enzyme-linked immunosorbent assay (ELISA) kits were provided by Jiangsu Maisha Industrial Co., Ltd., and included the following: Rat TNF-α ELISA Kit (Catalog No. MS-0180R1), Rat IL-10 ELISA Kit (Catalog No. MS-0195R1), Rat IL-1β ELISA Kit (Catalog No. MS-0047R1), and Rat IL-6 ELISA Kit (Catalog No. MS-0190R1). The Bone RNA Extraction Kit was procured from Beijing Biolaibo Technology Co., Ltd. (Catalog No. WM161005). Reverse transcription was performed using the Sunview® III Reverse Transcriptase Kit (with dsDNase, Catalog No. 1334606081), and Quantitative Polymerase Chain Reaction (qPCR) was carried out using the Sunview® SYBR qPCR SuperMix (Universal, Catalog No. 1174624162), both supplied by Shenzhen Shangwei Biotechnology Co., Ltd. Chloral hydrate for experimental use was obtained from Qingdao Yulong Seaweed Co., Ltd. (Batch No. 20120801).

2.3 Establishment of a collagen-induced arthritis (CIA) rat model

A total of 60 Sprague-Dawley rats (30 male and 30 female) were randomly assigned into six groups (n=10 per group, 5 males and 5 females per group) using a random number table method: the control group, model group, low-dose Dunhuang Mofeng ointment group, medium-dose group, high-dose group, and Voltaren group. The CIA model was established in the rats using bovine type II collagen combined with CFA or incom-

plete Freund's adjuvant. For model construction, bovine type II collagen (20 mg) was dissolved in 10 mL of 0.01 mol/L glacial acetic acid, prepared one day prior to the experiment, and stored overnight at 4 °C. On the day of initial immunization, the collagen solution was mixed at a 1:1 ratio with 10 mL of CFA and emulsified thoroughly using an oscillator until a uniform milky state was achieved. For the initial immunization, following intraperitoneal anesthesia with 6% chloral hydrate (6 mL/kg), rats received subcutaneous injections of 0.1 mL of the prepared emulsion at four sites: the dorsal region, 2 cm from the tail base, the lateral side of the right posterior ankle joint, and the right posterior foot. The total injected volume per rat was 0.4 mL. Rats in the control group received equivalent volumes of normal saline administered in the same manner. For the booster immunization, seven days after the initial immunization, a booster emulsion was prepared by mixing bovine type II collagen solution at a 1:1 ratio with incomplete Freund's adjuvant and emulsifying thoroughly. Under anesthesia, rats were injected subcutaneously with 0.1 mL of the emulsion at four sites: the dorsal region, 2 cm from the tail base, the lateral side of the left posterior ankle joint, and the left posterior foot. The total injected volume per rat was 0.4 mL. Model evaluation was performed on the seventh day following the booster immunization. Rats from the blank and model groups were randomly selected for X-ray imaging to assess the success rate of CIA model establishment.

2.4 Administration method and sample collection

Following successful model establishment, drug treatment was initiated, with dosages determined based on the principle of human-to-rat dose conversion as outlined in the Methodology of TCM Pharmacology Research. The experimental groups received the following interventions: the blank and model groups received no treatment; the Voltaren group received external application of Voltaren ointment; the low-dose, medium-dose, and high-dose groups were administered 5%, 10%, and 17% Dunhuang Mofeng ointment, respectively. In accordance with experimental protocols, the corresponding ointment was evenly applied to the ankle joints of the rats in each group. To prevent licking, medical tape was used to secure the ankle joints. The ointment was applied twice daily, between 08:00-09:00 and 20:00-21:00, for a duration of 7 weeks. Following the final dosing, rats were fasted for 24 hours, and samples were collected the subsequent day. Blood was drawn from the abdominal aorta, centrifuged at 3000 rpm for 15 minutes, and the serum was stored at ultra-low temperatures (-80 °C) for subsequent ELISA analysis. After euthanasia by decapitation, the right ankle tissues were rapidly frozen and stored at -80 °C for future qPCR analysis. All experimental measurements, including joint swelling, paw volume, and imaging assessments, were performed by investigators who were blinded to the group allocation.

2.5 Body weight measurement

The rat containment box was placed on an electronic balance and tared to zero. Subsequently, the body weight of each rat in all groups was measured sequentially prior to treatment and on days 7, 14, 21, 28, 35, 42, and 49 following the initiation of drug administration.

2.6 Measurement of right ankle joint diameter

Ankle joint swelling was assessed using a vernier caliper at predefined intervals: prior to treatment and on days 7, 14, 21, 28, 35, 42, and 49 following the initiation of drug administration. Measurements were systematically recorded, with the evaluation points defined as the upper edges of the medial and lateral malleoli.

2.7 Measurement of paw volume

Plantar volume was assessed using a plantar volume measurement instrument at baseline and on days 7, 14, 21, 28, 35, 42, and 49 following drug administration. Methodology: The right ankle joint of each rat was marked with a waterproof marker for consistency. The plantar volume measurement instrument was calibrated prior to use, and the right hind paw of each rat was immersed in a pre-prepared liquid within the measurement container. For each rat, measurements were performed twice, and the average value was recorded for analysis.

2.8 Computed radiography imaging

The right femoral shaft was excised, and computed radiography was performed using a current of 3.2 mA/s, a voltage of 40 kV, and a source-to-detector distance of 90 cm. Radiographic imaging was employed to evaluate callus continuity and fracture healing.

2.9 ELISA detection

Following drug intervention, the serum levels of TNF-α, IL-1β, IL-6, and IL-10 were quantified by ELISA. Serum samples from the treated rats in each group were centrifuged at 3000 rpm for 10 minutes, and the supernatant was carefully collected. Assays were conducted according to the ELISA kit instructions. The optical density at 450 nm was measured, and a standard curve was generated to calculate the concentrations of the relevant cytokines.

2.10 RT-qPCR detection

Total RNA was extracted from rat bone tissue using TRIzol reagent, and samples were stored at -80 °C for subsequent analysis. RT-qPCR was performed using the One Step TB Green PrimeScript RT-PCR Kit to detect the amplified products in

Table 1. Primer sequence information

Gene	GenBank number	Primer sequence	Product/bp
STAT1	NM_007315.4	F: TGTCTGAAGTCCACCCTTCTA R: GTCAAATTCAGAGCCCACTATCT	104
CCND1	NM_053056.3	F: CAACAACTTCCTCTCCTGCTAC R: GAAGGGCTTCAATCTGTTCCT	104
CDK4	NM_000075.4	F: CTTTGGCCTAGCCAGAATCTAC R: ACAGCCAACACTCCACATATC	133
GAPDH	NM_002046.7	F: ACAGCAACAGGGTGGTGGAC R: TTTGAGGGTGCAGCGAACTT	252
MYC	NM_002467.6	F: CTCGGTGCAGCCCTATTTCA R: TAGCGACCGCAACATAGGAC	185
CDKN1A	NM_000389.5	F: CCCGAGAACGGTGGAACTTT R: ACACCAGAGTGCAAGACAGC	231
MCL1	NM_021960.5	F: TTCTCGAGTGATGACCCATGT R: TCCCAGCCTCTTTGTTTCACA	201
FOS	NM_005252.4	F: GAGGGAGCTGACAGATACGC R: TCCAGGGAGGTCACAGACAT	192

real-time. The 20 μL reaction mixture comprised 2 μL of RNA sample, 10 μL of 2× One Step TB Green RT-PCR Buffer, and 0.8 μL of each 10 pmol forward and reverse primers. The reaction conditions included reverse transcription at 42 °C for 5 minutes, followed by denaturation at 95 °C for 10 seconds, and PCR amplification at 95 °C for 5 seconds, 60 °C for 34 seconds, for a total of 40 cycles. PCR products were analyzed using SDS v1.4 software. Gene-specific primers were synthesized by Lanzhou Kebao Co., Ltd. (China). Relative quantification was performed using the 2^−ΔΔCt method with GAPDH as the internal control. Data are presented as mean ± standard deviation (x±s). One-way analysis of variance was conducted using GraphPad Prism 7.0 software. The sequences of the upstream and downstream primers are listed in **Table 1**.

2.11 Extraction of active ingredients from TCM and related targets

In the TCMSP database, the keywords "Rhubarb", "Angelica", "Chuanxiong", "Croton", "Salvia miltiorrhiza", "Aconitum", and "Zanthoxylum" were used for querying. Screening criteria for active ingredient attributes were established based on the transdermal absorption characteristics of topical medications and the five drug classification principles, as follows: molecular weight (MW)≤500, the adipose-water partition coefficient (AlogP) between 1 and 3, and drug-likeness (DL)≥0.18. Active ingredients that met these criteria were selected from the TCMSP database. A file named "ingredients.txt" was created, and "Related Targets" was used to extract the target information for the TCM components. This information was stored in the "targets.txt" file. Using Perl, a script was executed to retrieve the active ingredients of the compound and their corresponding target data, generating a file named "allTargets.txt". The UniProtKB database, with a focus on Reviewed entries, was used to retrieve gene annotation files. The following conditions were applied: Status: Reviewed; Organism: Human. A script was run through Perl to transform the drug target identifiers (IDs) and obtain a file named "allTargets.symbol.txt", thereby constructing the target database for the active ingredients of the drug.

2.12 Identification of overlapping genes between RA-related targets and Dunhuang Mofeng ointment targets

Gene expression data associated with RA were retrieved from the GEO database, including datasets GSE56649, GSE15573, GSE93272, and GSE97779. Following normalization of the genetic data, differential genes were filtered based on |logFC|>1 and an adjusted p-value (adj. P.Val)<0.05. R software was employed to process the differential genes and identify the relevant targets of the active ingredients in Dunhuang Mofeng ointment. The intersection of these genes was then determined, enabling the preliminary identification of potential active ingredients and target proteins for the intervention of RA with Dunhuang Mofeng ointment.

2.13 Construction of the regulatory network diagram for Dunhuang Mofeng ointment

The active ingredients, targets, and RA-related differential genes of Dunhuang Mofeng ointment were systematically screened. Files, including "text file", "net.type.text", "net.geneLists.text", and "net.molLists.text", pertinent to the network regulation of TCM compounds, were generated by executing the Perl script. These files were subsequently imported into Cytoscape 3.8.0 software to construct the regulatory network diagram illustrating the "drug–active ingredient–target" interactions.

2.14 Construction of the protein-protein interaction (PPI) network and core target network diagram

The "disease-drug" common targets were imported into the STRING database, with the following settings: species set to *Homo sapiens* and a medium confidence threshold of 0.400. All other parameters remained at their default values, with free genes excluded. The preliminary PPI network was generated and exported as a TSV file for subsequent analysis in Cytoscape 3.8.0. Network topology analysis and visualization were conducted using the CytoNCA plugin, with the identification of the PPI network core based on metrics such as betweenness centrality, closeness centrality, degree centrality, eigenvector centrality, local average connectivity, and network centrality. The relevant core target proteins were filtered based on scores greater than the median by executing an R script on the resulting data.

2.15 Gene Ontology (GO) and Kyoto Encyclopedia of Genes and Genomes (KEGG) pathway enrichment analysis

The R script was executed to convert the symbols of the intersection genes between TCMtargets and RA into gene IDs. The following script parameters were applied: P-value filtering condition: pvalueFilter <0.05; corrected P-value filtering condition: qvalueFilter <0.05. GO functional enrichment and KEGG pathway enrichment analyses were performed. The GO analysis focused on the top 10 biological processes, cellular components, and molecular functions. KEGG pathway enrichment analysis highlighted the top 30 signaling pathways. Visualization was generated using histograms and bubble plots.

2.16 Molecular docking to validate the potential targets and active ingredients of Dunhuang Mofeng ointment in intervening RA

The two-dimensional structures of the small molecule ligands—luteolin, apigenin, quercetin, aloe-emodin, and emodin—representing the top five active ingredients identified in the previous analysis, were downloaded in SDF format from the PubChem database. Using Chem3D software, these structures were optimized and converted into three-dimensional models, which were subsequently saved in MOL2 format. Protein IDs corresponding to the core targets CCND1, MYC, CDKN1A, FOS, MCL1, STAT1, and CDK4 were retrieved from UniProt, and their three-dimensional structures were obtained from the Protein Data Bank (PDB). The receptor proteins were processed to remove water molecules, and small molecule ligands were prepared using PyMOL software. The protein receptor files were saved in PDB format. Hydrogens were added to the protein receptor files using AutoDockTools, and both the protein receptor (PDB format) and the small molecule ligands (MOL2 format) were converted into PDBQT format. To define the active pocket, a Grid Box was generated in AutoDockTools, with the center coordinates of the grid program being adjusted based on the receptor's binding site. Since the exact binding site was unknown, the size of the active pocket was optimized to allow maximum movement of the receptor and ligand during initial docking. The lattice spacing was set to 1 Å, and the dimensions (X, Y, Z) of the grid were determined. The center of the grid was placed at the presumed central region of the binding site, and all relevant parameters were saved in a grid.gpf file. Molecular docking was performed using AutoDock Vina software, with binding energy serving as the key parameter for evaluating ligand-receptor interactions. A binding energy threshold of ≤-5.0 kcal/mol was considered indicative of favorable binding. The docking results were visualized in both 2D and 3D using PyMOL and Discovery Studio software.

3 RESULTS

3.1 Effect of Dunhuang Mofeng ointment on ankle joint swelling in rats from different experimental groups

Compared to the control group, both the model and drug treatment groups exhibited bilateral ankle swelling, reduced mobility, and hair discoloration during both the primary and booster immunizations. On day 7 following the booster immunization, two rats from the control group and two from the model group were randomly selected for X-ray imaging (**Figure 2A-D**). The results revealed pronounced soft tissue edema in the bilateral ankle joints of the model group, with a marked narrowing of the ankle joint space, blurred joint boundaries, and evident bone destruction. Additionally, the appearance of the rats' feet was photographed prior to treatment and at subsequent time points (days 7, 14, 21, 28, 35, 42, and 49 post-treatment) for all experimental groups (**Figure 2E-J**). Compared to the control group, swelling and erythema of the ankle joint extending to the toe joint were observed in the other groups at various time points. In the model group, redness and swelling in the foot and ankle joints progressively worsened from days 7 to 35 post-administration, accompanied by joint deformity, stiffness, and restricted movement. In contrast, the Dunhuang Mofeng ointment (low, medium, and high-dose) groups and the Voltaren group showed a reduction in ankle and foot swelling and a noticeable decrease in erythema after 21 days of treatment. As the treatment period continued, swelling in the ankles and toes of rats in the drug groups gradually diminished. By day 49, joint redness and swelling were nearly completely resolved, with a significant improvement in joint mobility. These findings suggest that both Dunhuang Mofeng ointment and Voltaren have potential efficacy in alleviating symptoms of RA in this model.

3.2 Effect of Dunhuang Mofeng ointment on the body weight of rats in different experimental groups

Observation and analysis of body weight changes in rats across different experimental groups (**Figure 3A**; **Table 2**) revealed a normal growth trajectory in both the model and drug-treated groups prior to administration, with no significant differences compared to the control group. Throughout the entire experimental period (from pre-administration to day 49), the body weight of rats in all groups exhibited a consistent upward trend without any abnormal fluctuations. These findings indicate that the administration of Dunhuang Mofeng ointment did not exert any discernible effects on the body weight of the rats, demonstrating its favorable safety profile.

3.3 Effect of Dunhuang Mofeng ointment on the right ankle joint of rats in different experimental groups

The changes in the diameter of the right ankle joint across the experimental groups are presented in **Figure 3B** and **Table 3**.

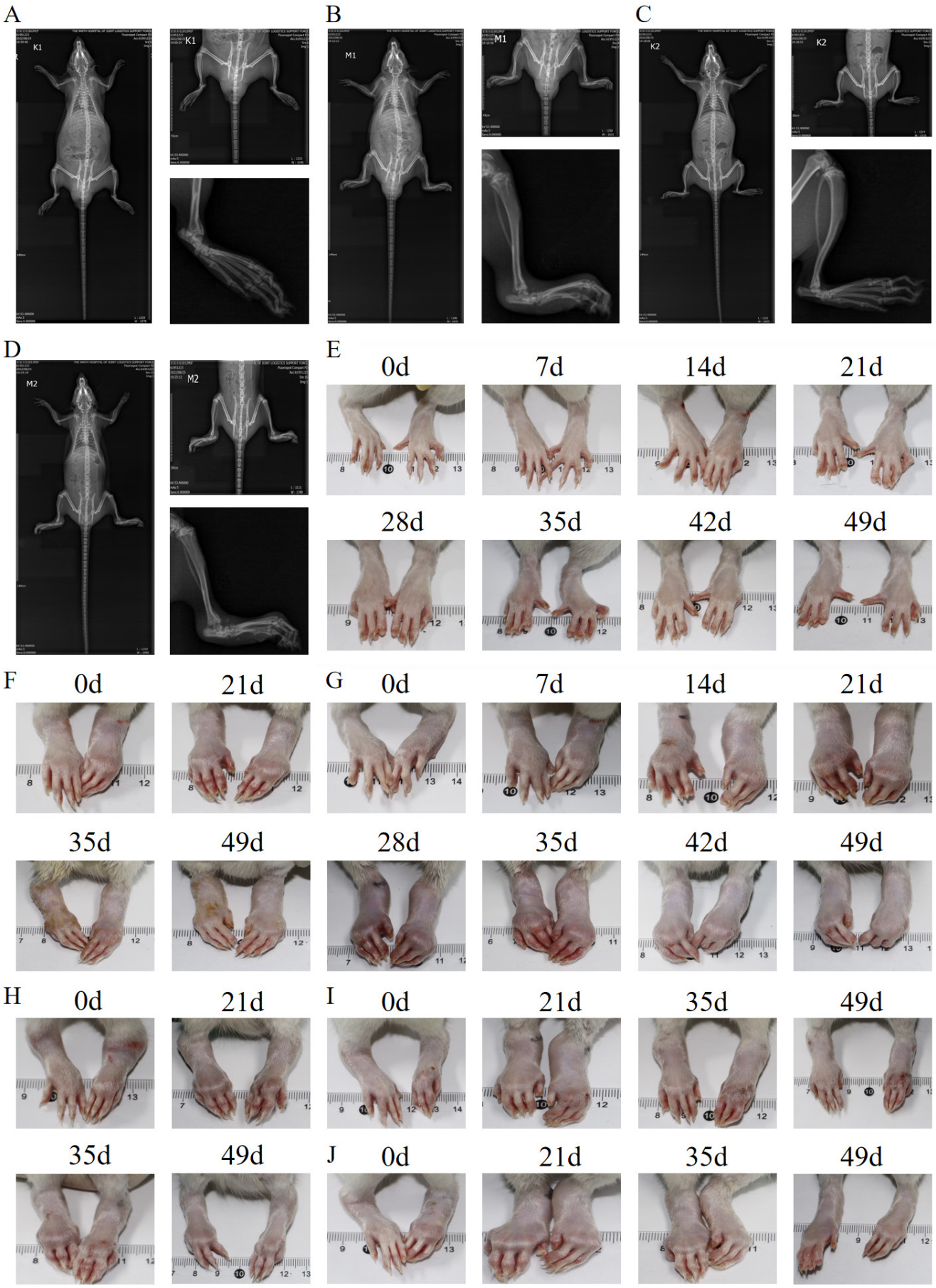
A
K1
K1
B
M1
M1
C
K2
K2
D
M2
M2
E
0d
7d
14d
21d
28d
35d
42d
49d
F
0d
21d
35d
49d
G
0d
7d
14d
21d
28d
35d
42d
49d
H
0d
21d
35d
49d
I
0d
21d
35d
49d
J
0d
21d
35d
49d

Figure 2. Radiographic changes and ankle joint swelling in rats across experimental groups. (A-D) Radiographic manifestations of rat ankle joints: A and C: control group, B and D: model group; (E-J) Swelling of the ankle joints in rats at different time points in each group: E: control group, F: high-dose drug intervention group, G: model group, H: Western medicine group (Voltaren), I: low-dose drug intervention group, J: medium-dose drug intervention group.

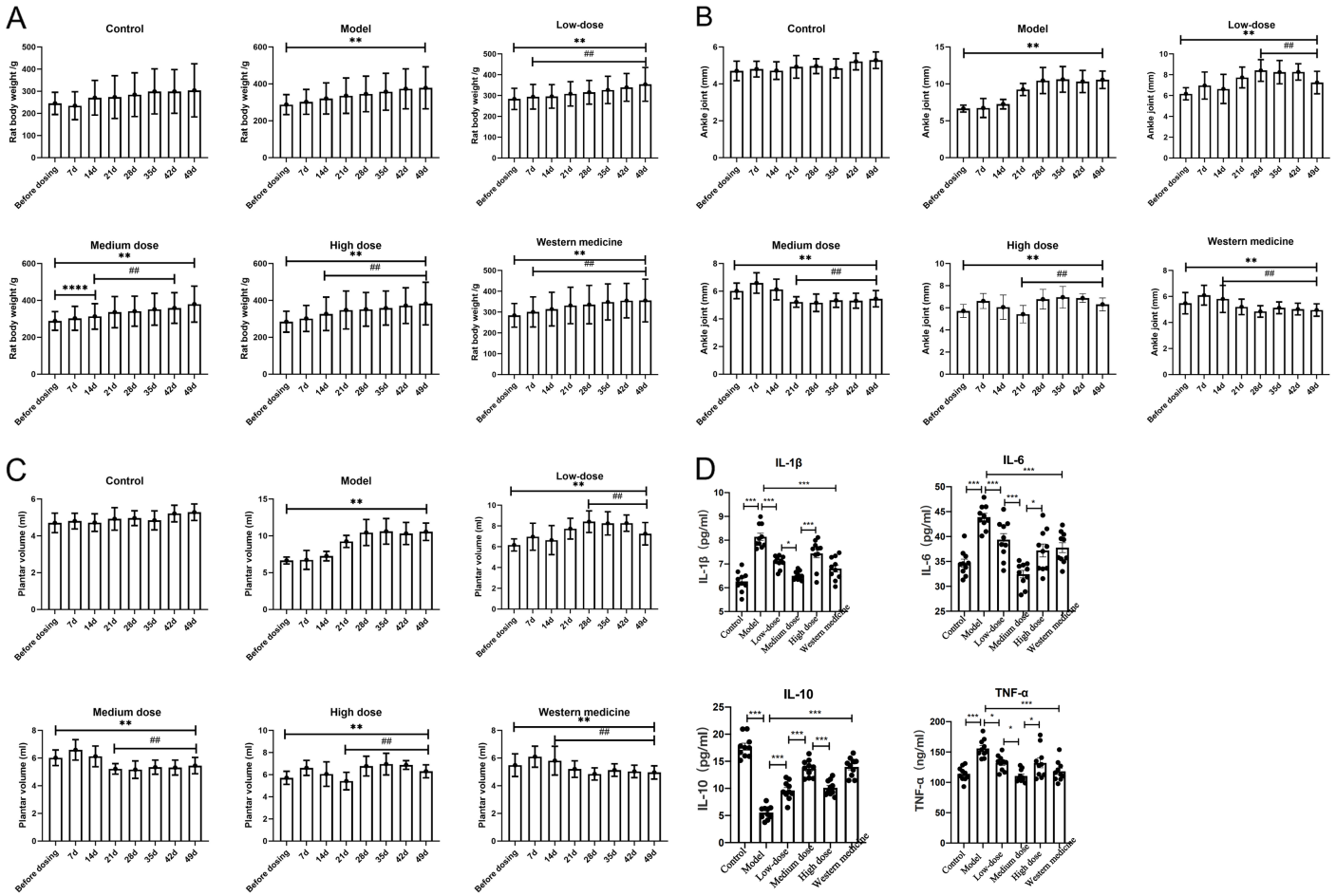

Figure 3. Effects of Dunhuang Mofeng ointment on body weight, ankle joint swelling, plantar volume, and serum inflammatory factors in rats. (A) Influence of Dunhuang Mofeng ointment on body weight of rats in different experimental groups; (B) Changes in the right ankle joint of rats; (C) Changes in plantar volume of rats; (D) Serum inflammatory factor content of rats in each group. Table: *P<0.05, **P<0.01 compared with blank group; $^{\#}$P<0.05, $^{\#\#}$P<0.01 compared with model group. Bar chart: *P<0.05, **P<0.01, ***P<0.001, ****P<0.0001.

Table 2. Body weight changes in rats across experimental groups (g, mean ± SD, n=10 per group)

Time (days)	Control	Model	Low-dose	Medium-dose	High-dose	Western medicine
Pre	245.10±50.24	287.60±54.25**	283.98±50.69**	288.39±50.69**	284.37±56.80**	284.52±56.76**
7	234.40±63.13	302.31±67.44**	294.27±59.10$^{**,\#\#}$	302.71±64.91**	301.95±70.92**	300.79±72.21$^{**,\#\#}$
14	270.50±78.39	320.80±84.52**	296.01±56.54$^{**,\#\#}$	313.02±69.26$^{****,\#\#}$	326.83±90.72$^{**,\#\#}$	314.42±80.68$^{**,\#\#}$
21	273.50±96.64	335.76±96.08**	308.40±58.42$^{**,\#\#}$	336.26±84.49$^{**,\#\#}$	347.74±102.88$^{**,\#\#}$	331.86±87.58$^{**,\#\#}$
28	284.20±98.77	345.30±96.54**	315.89±56.89$^{**,\#\#}$	341.43±81.27$^{**,\#\#}$	351.54±91.14$^{**,\#\#}$	335.97±92.07$^{**,\#\#}$
35	299.10±101.85	357.36±100.13**	326.93±65.65$^{**,\#\#}$	351.9±86.27$^{**,\#\#}$	358.38±92.34$^{**,\#\#}$	348.73±86.62$^{**,\#\#}$
42	299.00±98.86	373.04±108.13**	339.27±66.62$^{**,\#\#}$	358.69±82.85$^{**,\#\#}$	371.54±96.93$^{**,\#\#}$	355.18±82.69$^{**,\#\#}$
49	304.00±120.11	378.48±113.98**	353.79±81.15$^{**,\#\#}$	379.91±97.45**	382.79±115.43$^{**,\#\#}$	355.59±102.52$^{**,\#\#}$

Note: SD, standard deviation; **P<0.01, ****P<0.0001 compared with control group; $^{\#\#}$P<0.01 compared with model group.

Prior to treatment, the diameter of the right ankle joint in the model and all drug-treated groups was significantly increased compared to the control group (*P<0.01*), indicating the successful establishment of the model. In the model group, foot swell-

Table 3. Changes in right ankle joint diameter in each experimental group (mm, mean ± SD, n=10 per group)

Time (days)	Control	Model	Low-dose	Medium-dose	High-dose	Western medicine
Pre	4.70±0.53	6.65±0.47**	6.17±0.58**	6.02±0.56**	5.71±0.59**	5.48±0.82**
7	4.80±0.43	6.73±1.29**	6.96±1.30**	6.59±0.74**	6.61±0.68**	6.10±0.76**
14	4.72±0.48	7.25±0.64**	6.64±1.40**	6.12±0.75**	6.05±1.10**	5.81±1.04$^{**,\#\#}$
21	4.92±0.61	9.24±0.82**	7.74±1.00**	5.22±0.38$^{**,\#\#}$	5.42±0.79$^{**,\#\#}$	5.20±0.60$^{**,\#\#}$
28	4.96±0.40	10.45±1.77**	8.41±1.04$^{**,\#\#}$	5.16±0.63$^{**,\#\#}$	6.77±0.89$^{**,\#\#}$	4.85±0.44$^{**,\#\#}$
35	4.84±0.52	10.61±1.74**	8.25±1.12$^{**,\#\#}$	5.34±0.51$^{**,\#\#}$	6.95±0.98$^{**,\#\#}$	5.13±0.45$^{**,\#\#}$
42	5.21±0.45	10.32±1.50**	8.27±0.78$^{**,\#\#}$	5.31±0.54$^{**,\#\#}$	6.87±0.39$^{**,\#\#}$	5.03±0.45$^{**,\#\#}$
49	5.28±0.45	10.55±1.18**	7.25±1.08$^{**,\#\#}$	5.45±0.59$^{**,\#\#}$	6.30±0.59$^{**,\#\#}$	4.96±0.48$^{**,\#\#}$

Note: SD, standard deviation; **P<0.01 compared with control group; $^{\#\#}$P<0.01 compared with model group.

Table 4. Changes in right paw volume in each experimental group (mL, mean ± SD, n=10 per group)

Time (days)	Control	Model	Low-dose	Medium-dose	High-dose	Western medicine
Pre	1.76±0.25	2.54±0.41**	2.54±0.34**	2.62±0.44**	2.65±0.30**	2.65±0.26**
7	1.66±0.30	3.37±0.67**	3.37±1.10**	2.98±0.47$^{**,\#\#}$	3.03±0.46$^{**,\#\#}$	3.01±0.35$^{**,\#\#}$
14	1.70±0.41	3.50±0.41**	3.76±1.13$^{**,\#\#}$	3.08±0.58$^{**,\#\#}$	3.03±0.56$^{**,\#\#}$	2.98±0.49$^{**,\#\#}$
21	1.70±0.50	3.16±0.44**	3.35±0.95$^{**,\#\#}$	2.97±0.55$^{**,\#\#}$	3.02±0.60$^{**,\#\#}$	2.89±0.52$^{**,\#\#}$
28	1.59±0.44	2.99±0.29**	3.21±0.76$^{**,\#\#}$	2.86±0.47$^{**,\#\#}$	3.01±0.71**	2.76±0.57$^{**,\#\#}$
35	1.71±0.42	3.05±0.51**	2.78±0.64$^{**,\#\#}$	2.83±0.49$^{**,\#\#}$	2.85±0.65$^{**,\#\#}$	2.66±0.44$^{**,\#\#}$
42	1.79±0.33	3.04±0.54**	3.16±0.67$^{**,\#}$	2.80±0.42$^{**,\#\#}$	2.97±0.72$^{**,\#\#}$	2.50±0.43$^{**,\#\#}$
49	1.77±0.36	2.94±0.52**	3.06±0.73$^{**,\#}$	2.85±0.55$^{**,\#\#}$	2.99±0.65**	2.80±0.55$^{**,\#\#}$

Note: SD, standard deviation; **P<0.01 compared with control group; $^{\#}$P<0.05, $^{\#\#}$P<0.01 compared with model group.

ing progressively worsened, with the right ankle diameter remaining markedly higher than that of the control group at day 35 post-administration (*P<0.01*). Although a gradual reduction in ankle diameter was observed in the model group by day 42, the difference from the control group remained statistically significant (*P<0.01*). In contrast, the drug-treated groups exhibited a significant reduction in ankle joint diameter by day 28 (*P<0.01*), indicating that both Dunhuang Mofeng ointment and Voltaren effectively alleviated ankle joint swelling and mitigated inflammation-related symptoms.

3.4 Effect of Dunhuang Mofeng ointment on paw volume in rats from different experimental groups

The changes in right plantar volume across the experimental groups are illustrated in **Figure 3C** and **Table 4**. Prior to treatment, the right plantar volume in the model group and all drug-treated groups was significantly elevated compared to the control group (*P<0.01*), further supporting the successful establishment of the model. During the treatment period, the right plantar volume in the model group exhibited a slight reduction by day 21, but it remained significantly higher than that of the control group (*P<0.01*). In contrast, all drug-treated groups demonstrated a downward trend in plantar volume by day 14 of administration; however, significant differences from the control group persisted (*P<0.01*). These findings suggest that both Dunhuang Mofeng ointment and Voltaren contributed to the alleviation of foot swelling, although complete resolution to normal levels was not achieved.

3.5 Effect of Dunhuang Mofeng ointment on inflammatory factors in rats from different experimental groups

ELISA analysis of serum biomarkers in rats across the experimental groups (**Figure 3D**) revealed that, compared to the control group, serum levels of TNF-α, IL-1β, and IL-6 were markedly elevated in the model group (*P<0.001*), while IL-10 levels were significantly reduced (P<0.001), confirming the successful induction of a robust inflammatory response. In contrast, treatment with both Dunhuang Mofeng ointment and Voltaren resulted in significant reductions in the serum levels of TNF-α, IL-1β, and IL-6 (*P<0.05*), alongside a notable increase in IL-10 expression (*P<0.001*) when compared to the model group. These results suggest that both treatments effectively modulate immune responses and mitigate inflammation.

3.6 Active components of TCM and their corresponding targets

In the TCMSP database, a total of 76 active ingredients were selected based on the screening criteria of "MW≤500, AlogP: 1-3, DL≥0.18". These included 13, 10, 1, 1, 39, 8, and 4 components derived from *Rheum officinale*, *Angelica sinensis*, *Ligusticum chuanxiong*, *Croton tiglium*, *Salvia miltiorrhiza*, *Zanthoxylum bungeanum*, and *Aconitum carmichaelii*, respec-

Table 5. Active ingredients of Dunhuang Mofeng ointment

Herb	MOL ID	Molecule name	MW	AlogP	DL
Rheum officinale	MOL001729	Crysophanol	254.25	2.76	0.21
	MOL002235	Eupatin	360.34	1.99	0.41
	MOL002249	Gallocatechin	306.29	1.65	0.27
	MOL002258	Physcion-9-O-beta-D-glucopyranoside_qt	300.28	2.48	0.30
	MOL002268	Rhein	284.23	1.88	0.28
	MOL002281	Toralactone	272.27	2.25	0.24
	MOL002286	Laccaic Acid D	300.23	1.61	0.31
	MOL002289	Physcione	284.28	2.15	0.27
	MOL002302	RHAPONTIN	406.42	1.26	0.55
	MOL000471	Aloe-emodin	270.25	1.67	0.24
	MOL000472	Emodin	270.25	2.49	0.24
	MOL000476	Physcion	284.28	2.74	0.27
	MOL000096	(-)-Catechin	290.29	1.92	0.24
Angelica sinensis	MOL005786	Byakangelicin	334.35	1.70	0.35
	MOL005789	Neobyakangelicol	316.33	2.72	0.31
	MOL005790	5-[[(2S)-3,3-dimethyloxiran-2-yl]methoxy]-3,7-dihydropyrano[3,2-f] benzofuran-2-one	288.32	1.47	0.31
	MOL005791	Oxypeucedanin	286.30	2.00	0.30
	MOL005792	{5-[2'(R)-Hydroxy-3'-methyl-3'-butenyl-oxy]furocoumarin}	286.30	2.74	0.26
	MOL005793	9-[[(2R)-3,3-dimethyloxiran-2-yl]methoxy]furo[3,2-g]chromen-7-one	286.30	2.49	0.29
	MOL005800	Byakangelicol	316.33	2.47	0.36
	MOL005806	4-[(2S)-2,3-dihydroxy-3-methylbutoxy]furo[3,2-g]chromen-7-one	304.32	1.72	0.29
	MOL005807	Sen-Byakangelicol	386.43	2.76	0.61
	MOL013430	Prangenin	286.30	2.49	0.29
Ligusticum chuanxiong	MOL001729	Crysophanol	254.25	2.76	0.21
Croton tiglium	MOL001626	Phrymarolin-II	458.45	2.30	0.93
Salvia miltiorrhiza	MOL000569	Digallate	322.24	1.53	0.26
	MOL000006	Luteolin	286.25	2.07	0.25
	MOL006452	1,5-Dihydroxy-3-methylanthraquinone	254.25	2.76	0.21
	MOL007040	1-ketoisocryptotanshinone	310.37	2.59	0.44
	MOL007053	7-oxoroyleanone	330.46	3.00	0.34
	MOL007063	Przewalskin A	398.49	2.25	0.65
	MOL007068	Przewaquinone B	292.30	2.99	0.41
	MOL007070	(6S,7R)-6,7-dihydroxy-1,6-dimethyl-8,9-dihydro-7H-naphtho[8,7-g] benzofuran-10,11-dione	312.34	2.34	0.45
	MOL007071	Przewaquinone F	312.34	2.07	0.46
	MOL007080	Tanshinol A	292.30	2.99	0.41
	MOL007081	Danshenol B	354.48	2.59	0.56
	MOL007082	Danshenol A	336.41	2.01	0.52
	MOL007090	Danshexinkum A	296.34	2.59	0.30
	MOL007093	Danshexinkum D	336.41	2.83	0.55
	MOL007100	Dihydrotanshinlactone	266.31	2.77	0.32
	MOL007101	DihydrotanshinoneI	278.32	2.86	0.36
	MOL007105	Epidanshenspiroketallactone	284.38	2.37	0.31
	MOL007116	Methylrosmarinate	374.37	2.94	0.37
	MOL007120	Miltionone II	312.39	2.14	0.44
	MOL007121	Miltipolone	300.43	2.74	0.37
	MOL007128	Paramiltioic Acid	332.43	2.68	0.37

	MOL007129	Potassium Salvianolate D	418.38	2.33	0.50
	MOL007130	Prolithospermic Acid	314.31	2.77	0.31
	MOL007131	(2S,3S)-2-(3,4-dihydroxyphenyl)-7-hydroxy-4-[(E)-3-hydroxy-3-oxoprop-1-enyl]-2,3-dihydrobenzofuran-3-carboxylic acid	358.32	2.07	0.41
	MOL007132	(2R)-3-(3,4-dihydroxyphenyl)-2-[(Z)-3-(3,4-dihydroxyphenyl)acryloyl]oxy-propionic acid	360.34	2.69	0.35
	MOL007133	Salviacoccin	356.40	1.41	0.63
	MOL007135	Salvianic Acid C	378.36	2.03	0.37
	MOL007138	Salvianolic Acid D	418.38	2.33	0.50
	MOL007140	(Z)-3-[2-[(E)-2-(3,4-dihydroxyphenyl)vinyl]-3,4-dihydroxy-phenyl] acrylic acid	314.31	2.82	0.26
	MOL007141	Salvianolic Acid G	340.30	2.20	0.61
	MOL007143	Salvilenone I	270.40	2.88	0.23
	MOL007150	(6S)-6-hydroxy-1-methyl-6-methylol-8,9-dihydro-7H-naphtho[8,7-g] benzofuran-10,11-quinone	312.34	2.42	0.46
	MOL007151	Tanshindiol B	312.34	2.34	0.45
	MOL007152	Przewaquinone E	312.34	2.34	0.45
	MOL007156	Tanshinone VI	296.34	2.44	0.30
	MOL000008	Apigenin	270.25	2.33	0.21
Aconitum carmichaelii	MOL002384	14-Deoxy-11,12-didehydroandrographolide	332.48	2.10	0.32
	MOL002388	Delphin_qt	303.26	1.67	0.28
	MOL002392	Deltoin	328.39	2.48	0.37
	MOL002398	Karanjin	292.30	2.94	0.34
	MOL002414	Denudatine	343.56	2.25	0.67
	MOL002419	(R)-Norcoclaurine	271.34	2.57	0.21
	MOL002421	Ignavine	449.59	1.22	0.25
	MOL002436	Delavaconitine	497.69	1.38	0.37
Zanthoxylum bungeanum	MOL013271	Kokusaginin	259.28	2.33	0.20
	MOL002663	Skimmianin	259.28	2.33	0.20
	MOL002881	Diosmetin	300.28	2.32	0.27
	MOL000098	Quercetin	302.25	1.50	0.28

Note: MOL ID, molecule identifier; MW, molecular weight; AlogP, adipose-water partition coefficient; DL, drug-likeness.

tively. After eliminating duplicates, 75 unique active ingredients remained (see **Table 5**). Additionally, the drug targets associated with the Dunhuang Mofeng ointment were extracted from the TCMSP database, yielding a total of 908 potential targets. These targets were standardized using the UniProt database, applying the "Human" and "Reviewed" filters, and subsequently converted to standardized gene names. After removing duplicates, a final set of 85 distinct target genes was identified.

3.7 Intersection genes between RA differential genes and Dunhuang Mofeng ointment-related targets

Gene expression datasets associated with RA were obtained from the GEO database, including GSE15573, GSE56649, GSE93272, and GSE97779. The data were preprocessed and normalized using R software, followed by differential gene expression analysis conducted using the limma package. The filtering criteria included |logFC|>1 and adjusted P-value <0.05. Based on these criteria, both upregulated and downregulated differential genes were identified (**Figure 4A**). Specifically, in the GSE15573 dataset, 22 differential genes were identified, of which 21 were upregulated and 1 was downregulated. In the GSE56649 dataset, a total of 724 differential genes were identified, with 409 upregulated and 315 downregulated. The GSE93272 dataset yielded 26 differential genes, 25 of which were upregulated and 1 downregulated. In the GSE97779 dataset, 2792 differential genes were identified, comprising 1240 upregulated genes and 1552 downregulated genes. A heatmap illustrating the expression profiles of these differential genes is shown in **Figure 4B**. After removing duplicates, a total of 3564 unique differential genes were identified, of which 3397 were selected for further analysis (**Figure 4C**). Additionally, intersection analysis between drug targets and RA-related differential genes was performed using R software, revealing 21 intersecting genes: ADRB2, CDKN1A, BAX, TNF, MYC, ACTA2, CCND1, RB1, CDK4, MCL1, COLQ, FOS, RUNX1T1, CCND2, PSMD3, FCER2, TRPM2, STAT1, CXCL11, CXCL10, and SPP1. These intersection genes are depicted in a Venn diagram (**Figure 4D**).

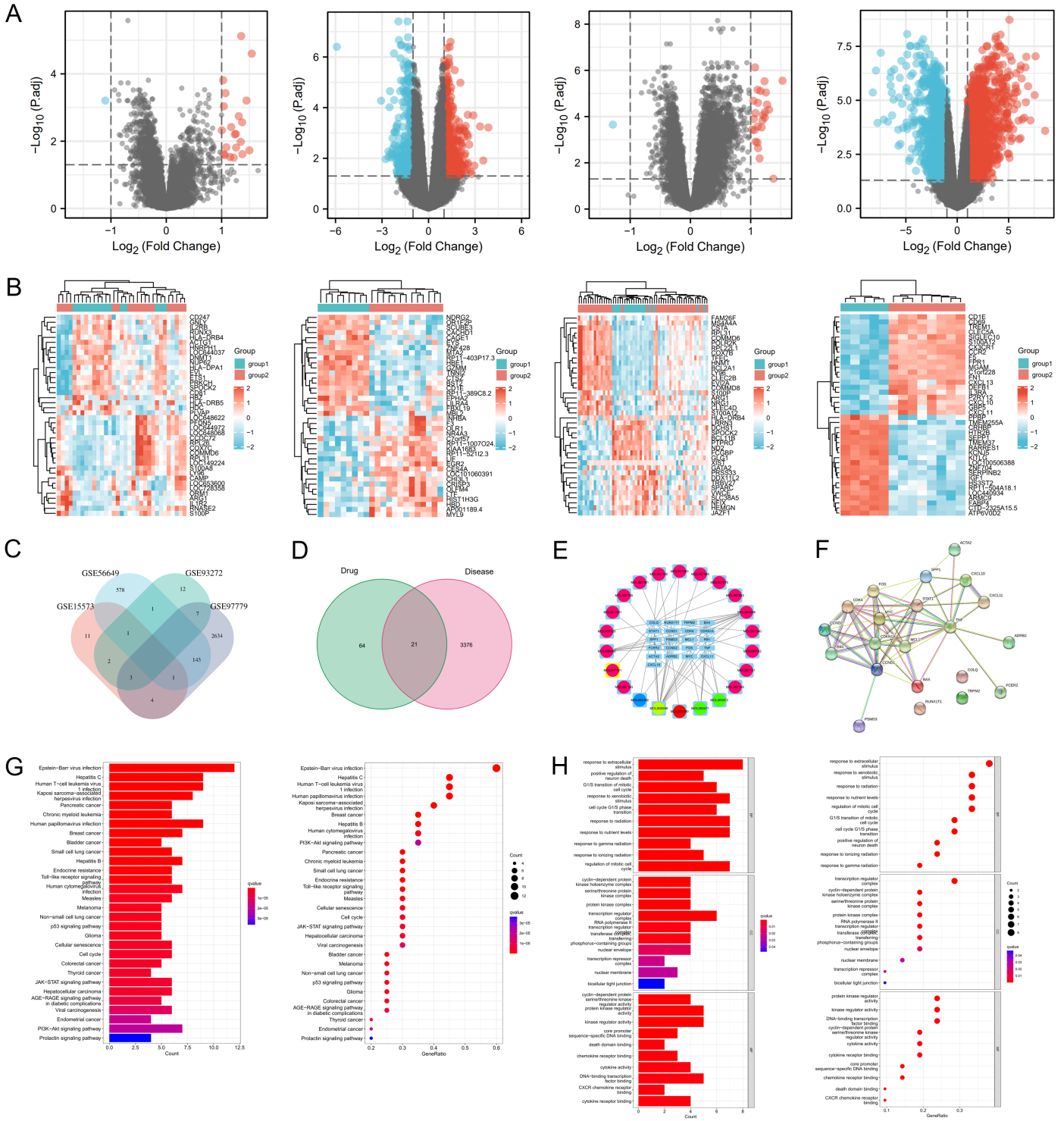

Figure 4. Identification of key targets and pathways of Dunhuang Mofeng ointment in RA based on differential gene and network pharmacology analysis. (A) Volcano plot of differential genes in RA-related gene datasets GSE15573, GSE56649, GSE93272 and GSE97779; (B) Heat maps of differential genes in GSE15573, GSE56649, GSE93272, and GSE97779; (C) Intersection of differential genes across GSE15573, GSE56649, GSE93272, and GSE97779; (D) Intersection genes between Dunhuang Mofeng ointment targets and RA-related genes; (E) Regulatory network of Dunhuang Mofeng ointment active ingredients and their targets; (F) PPI network and core targets of Dunhuang Mofeng ointment in RA treatment; (G) KEGG pathway enrichment analysis; (H) GO functional enrichment analysis. RA, rheumatoid arthritis; PPI, protein-protein interaction; KEGG, Kyoto Encyclopedia of Genes and Genomes; GO, Gene Ontology.

Table 6. Core PPI network topology parameters

Name	Betweenness	Closeness	Degree	Eigenvector	LAC	Network
CCND1	44.07	0.773	24	0.345	12.67	18.80
MYC	12.07	0.739	22	0.341	13.82	18.93
CDKN1A	7.41	0.708	20	0.323	14.00	17.57
FOS	9.04	0.708	20	0.322	13.60	16.64
MCL1	3.86	0.680	18	0.302	13.33	15.32
STAT1	16.24	0.680	18	0.277	10.67	13.10
CDK4	5.05	0.680	18	0.304	13.78	15.66

Note: PPI, protein-protein interaction; LAC, local average connectivity.

Table 7. Binding energy of core active ingredients and core protein targets

Protein	PDB ID	Ligand	Grid_size	Affinity (kcal/mol)
CCND1	2w96	Luteolin	66*52*78	-9.0
CCND1	2w96	Apigenin	64*52*76	-8.7
CCND1	2w96	Quercetin	64*52*86	-9.4
MYC	5i4z	Aloe-emodin	98*48*40	-6.7
MYC	5i4z	Emodin	98*48*40	-6.5
MYC	5i4z	Quercetin	98*48*40	-6.3
CDKN1A	6cej	Aloe-emodin	40*40*40	-4.9
CDKN1A	6cej	Emodin	40*40*40	-5.0
CDKN1A	6cej	Luteolin	40*40*40	-5.8
CDKN1A	6cej	Apigenin	40*40*40	-5.4
CDKN1A	6cej	Quercetin	40*40*40	-5.7
MCL1	3mk8	Luteolin	40*40*40	-6.8
MCL1	3mk8	Apigenin	40*40*40	-6.5
STAT1	3wwt	Quercetin	54*40*70	-7.5
FOS	1a02	Apigenin	70*64*84	-8.1
FOS	1a02	Quercetin	76*64*86	-8.1
CDK4	3g33	Luteolin	112*98*94	-8.7
CDK4	3g33	Apigenin	112*96*80	-8.4

Note: PDB ID, Protein Data Bank identifier.

3.8 Construction of the regulatory network diagram for the Dunhuang Mofeng ointment formula

The data files pertaining to the network regulation of TCM compounds, obtained through Perl script execution, were imported into Cytoscape 3.8.0 for further analysis. A "drug - active ingredient - target" regulatory network was constructed (**Figure 4E**). In this network, light blue rectangular nodes represent the targets, while circular nodes denote the active ingredients of TCM. The edges connecting the nodes indicate that an active ingredient can modulate the corresponding RA-related target, with the line density reflecting the strength of the interaction. The top five active ingredients, ranked by the number of interactions, are as follows: MOL000098 (quercetin), interacting with 15 targets; MOL000008 (apigenin), interacting with 13 targets; MOL000006 (luteolin), interacting with 6 targets; MOL000471 (aloe-emodin), interacting with 4 targets; and MOL000472 (emodin), also interacting with 4 targets. Each active ingredient exhibits both independent regulatory effects and shared targets.

3.9 PPI network and core target analysis of Dunhuang Mofeng ointment in treating RA

The 21 "drug-disease" common targets were input into the STRING database to retrieve protein interaction data, and the resulting "string_interactions.tsv" file was downloaded. This file was subsequently imported into Cytoscape software, where the CytoNCA plugin was employed to calculate the network parameters of each protein, generating the scoring file "score1.csv". The R script was used to filter the "score1" file based on the following parameters: betweenness =2.63, closeness =0.60, degree =13, eigenvector =0.23, local average connectivity =9.71, and network =11.75. By applying these criteria, the core target proteins were identified as CCND1, MYC, CDKN1A, FOS, MCL1, STAT1, and CDK4. The topological parameters of these core proteins are ranked according to the degree score and presented in **Table 6** and **Figure 4F**.

3.10 GO enrichment and KEGG pathway analysis

GO enrichment analysis was performed using R software, yielding 1036 GO terms. The top 10 terms in each GO category (biological process, cellular component, and molecular function) were selected and visualized as bar and bubble charts (**Figure 4H**). Biological process enrichment showed thattargets were primarily involved in response to extracellular stimulus, G1/S transition of mitotic cell cycle, response to radiation, and regulation of the mitotic cell cycle. Cellular component enrichment indicated that target proteins were mainly localized in the cyclin-dependent protein kinase holoenzyme complex, serine/threonine protein kinase complex, transcription regulator complex, nuclear envelope, and bicellular tight junction. Molecular function enrichment revealed that targets was primarily associated with cyclin-dependent protein serine/threonine kinase regulator activity, protein kinase regulator activity, cytokine activity, and chemokine receptor binding. KEGG pathway enrichment analysis was performed using R software, identifying 90 signaling pathways. The top 30 significantly enriched pathways were selected and visualized as a bubble plot (**Figure 4G**). The results showed that the target was mainly enriched in the AGE-RAGE, JAK-STAT, PI3K-Akt, Toll-like receptor, and p53 signaling pathways, as well as pathways related to cellular senescence, cell cycle, cancer, viral infection, and diabetic complications.

3.11 Molecular docking

Molecular docking of small molecule ligands with protein receptors was performed using AutoDock Vina, and the docking results were evaluated based on affinity values (**Table 7**).

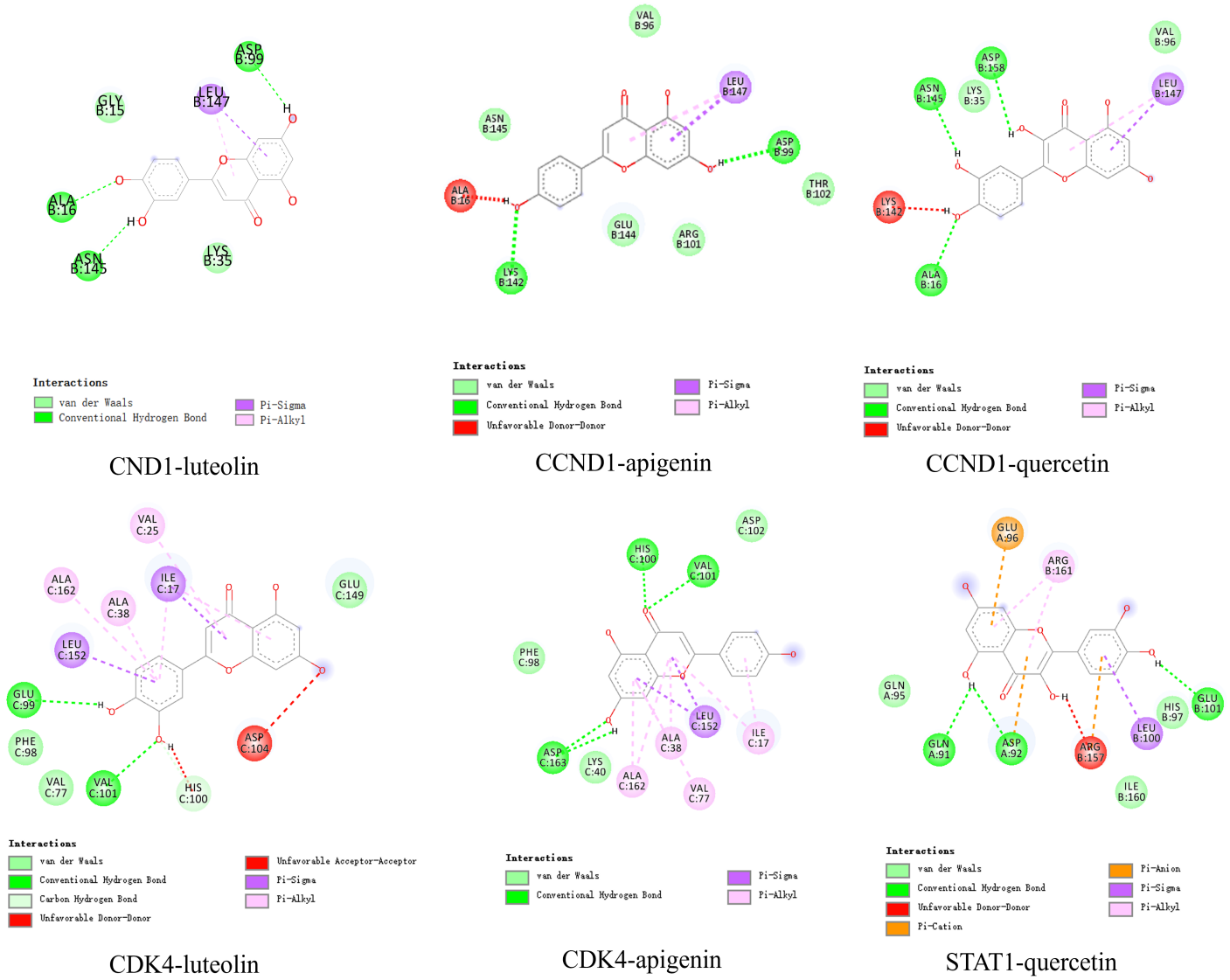

Figure 5. Molecular docking analysis of key targets and active compounds of Dunhuang Mofeng ointment.

The molecular docking results showed that the active compounds formed stable interaction networks with multiple target proteins within the binding pockets. Specifically, the ligands were able to form stable interactions with key amino acid residues (such as ASP, ASN, LYS, GLU, and HIS) through conventional hydrogen bonds, while also engaging in various non-covalent interactions including π–sigma, π–alkyl, and van der Waals interactions, which further enhanced the stability of ligand–protein binding. In addition, unfavorable donor–donor interactions and other weak interactions were observed in some complexes, suggesting a certain degree of conformational adaptability of the ligands within the binding sites. Overall, these multiple intermolecular interactions collectively contribute to maintaining the stable binding of the ligands within the active pockets of the target proteins, providing a structural basis for their potential biological activities (**Figure 5**).

3.12 mRNA expression levels of STAT1, CDK4, CCND1, MYC, CDKN1A, MCL1, and FOS in ankle joints of rats from different experimental groups

Compared to the control group, the mRNA expression levels of STAT1, CDK4, CCND1, MCL1, FOS, and MYC in the ankle joints of rats in the model group were significantly elevated ($P<0.001$), whereas the mRNA expression of CDKN1A was significantly reduced ($P<0.001$). In contrast, rats in all drug-treated groups exhibited significantly lower mRNA expressions of STAT1, CDK4, CCND1, MCL1, FOS, and MYC ($P<0.05$) compared to the model group, while CDKN1A mRNA expression was markedly increased ($P<0.001$). Notably, the medium-dose and Western medicine groups showed the most pronounced effects (**Figure 6**).

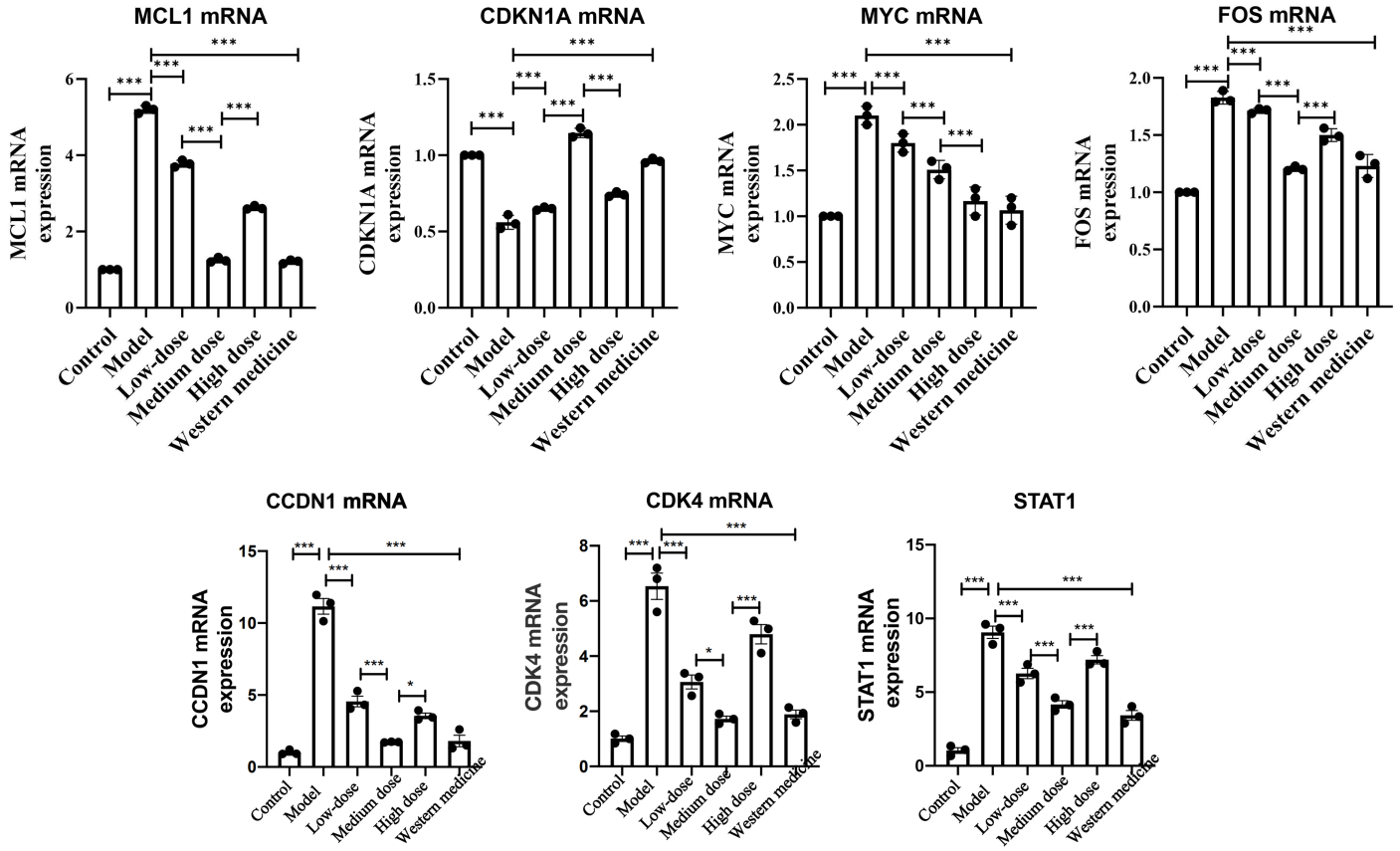

Figure 6. mRNA expression levels of target genes in the right ankle joint of rats in each group. *P<0.05, **P<0.01, ***P<0.001.

4 DISCUSSION

This study elucidates the potential mechanisms underlying the therapeutic effects of Dunhuang Mofeng ointment in the intervention of RA through network pharmacological analysis. The findings identify quercetin, apigenin, luteolin, aloe-emodin, and emodin as the key active ingredients of the formulation. RA, a chronic autoimmune disease, is characterized by joint inflammation, progressive damage, and, in severe cases, disability or mortality. Among these compounds, quercetin, a natural flavonoid with diverse biological activities, plays a pivotal role in RA management. Quercetin demonstrates pronounced anti-inflammatory and protective effects through multiple mechanisms. Studies indicate that quercetin can reverse neurodegenerative processes in the enteric nervous system and exhibit cytoprotective, genoprotective, and hepatoprotective properties [11]. In the context of RA, quercetin ameliorates inflammatory responses by modulating neutrophil activity, including inhibiting neutrophil infiltration, reducing plasma inflammatory cytokine levels, and promoting the apoptosis of activated neutrophils. Furthermore, it decreases the formation of neutrophil extracellular traps by suppressing autophagy, positioning quercetin as a promising candidate for RA treatment [12]. Clinical trials support these findings, revealing that an 8-week supplementation with quercetin significantly alleviated morning stiffness, morning pain, and post-activity pain in RA patients ($p<0.05$). Disease Activity Score and Health Assessment Questionnaire scores were markedly lower in the quercetin group compared to the placebo group, with a notable reduction in the proportion of patients exhibiting active disease. Additionally, plasma levels of high-sensitivity TNF-α were significantly reduced ($p<0.05$). Although no significant effect on erythrocyte sedimentation rate was observed ($p>0.05$), the number of tender joints was significantly decreased [13]. Mechanistic studies further highlight quercetin's multi-target regulatory potential. Quercetin mitigates IL-17-mediated activation of mTOR, extracellular signal-regulated kinase (ERK), and IκB-α pathways, thereby inhibiting osteoclastogenesis in RA. It also reduces RANKL expression in IL-17-induced RA synovial fibroblasts (RA-FLS), attenuating osteoclast differentiation. Moreover, quercetin regulates inflammatory responses in RA by inhibiting Th17 cell differentiation and IL-17 production, while sparing regulatory T cells [14]. In conclusion, quercetin, as a principal active ingredient of Dunhuang Mofeng ointment, exhibits a multi-target, multi-mechanism mode of action, offering a robust theoretical foundation and novel directions for the development of therapeutic agents for RA.

Apigenin, a natural flavonoid with chemopreventive properties, demonstrates significant pro-apoptotic activity across various

cell types. Studies have revealed that apigenin markedly inhibits TRAIL-induced proliferation of RA-FLS while restoring the expression of cell cycle inhibitors p21 and p27 [15]. This inhibitory effect is mediated through disruption of TRAIL-induced activation of the PI3K/Akt signaling pathway. Additionally, apigenin treatment triggers activation of MAPK ERK1/2, with pre-treatment using the ERK inhibitor PD98059 significantly attenuating apigenin-induced apoptosis. Apigenin-induced ERK1/2 activation and apoptosis are closely associated with the generation of intracellular ROS, a process that can be abrogated by the antioxidant Tiron, which blocks ROS production, ERK1/2 phosphorylation, and apoptotic cell death [16]. High-performance liquid chromatography analysis confirmed that the PEG-MSN carrier prolongs the half-life and enhances the stability of luteolin in vivo. Both luteolin and its nanocomplexes significantly suppress the expression of inflammatory markers, including TNF-α, IL-6, IL-1β, and IL-17. Histopathological evaluations corroborate these findings, showing reduced inflammatory cell infiltration, synovial hyperplasia, and joint destruction. Furthermore, luteolin inhibits the expression of key inflammatory targets, including P2X4, NLRP1, ASC, and Caspase-1 p10, highlighting its potent anti-inflammatory and joint-protective properties [17]. In conclusion, apigenin and luteolin exhibit substantial anti-RA potential via multi-target and multi-pathway modulation of inflammation and apoptosis. Their pharmacokinetic profiles can be further optimized through nanocarrier technologies, offering robust theoretical support and promising candidates for the prevention and treatment of RA.

Aloe-emodin effectively suppresses the production of nitric oxide, IL-6, and IL-1β in RAW264.7 cells stimulated by LPS, without inducing significant cytotoxic effects. Concurrently, the mRNA expression levels of iNOS, IL-6, and IL-1β were markedly downregulated. Western blot analysis further demonstrated that aloe-emodin attenuated LPS-induced iNOS protein expression, IκBα degradation, and the phosphorylation of ERK, p38, JNK, and Akt [18]. Emodin, another active compound, exhibits bidirectional immunomodulatory effects in RA by modulating the secretion of both pro-inflammatory cytokines (e.g., TNF-α, IL-6, IL-1β, and IL-17) and anti-inflammatory cytokines (e.g., IL-4, IL-10, and TGF-β), thereby inhibiting inflammation while promoting tissue repair [19]. Furthermore, emodin alleviates inflammatory arthritis, such as adjuvant-induced arthritis, by reducing neutrophil infiltration, promoting neutrophil apoptosis, and inhibiting autophagy and the formation of neutrophil extracellular traps [20]. These findings underscore the significant anti-inflammatory and anti-RA potential of emodin.

Molecular docking studies revealed that the active components of Dunhuang Mofeng extract, including aloe-emodin, exhibit strong binding affinities (binding energy ≤-5 kcal/mol) to key RA-related targets, such as CCND1, MYC, CDKN1A, FOS, MCL1, STAT1, and CDK4. Notably, the binding energy for CDKN1A was calculated at -4.9 kcal/mol. Overexpression of CCND1 and CDK4, coupled with the downregulation of p27, constitutes a pivotal molecular event in RA pathogenesis [21]. Additionally, CIP2A has been identified as a promoter of RA progression by enhancing synovial cell resistance to apoptosis, independent of c-Myc expression [22]. Under acidic conditions, activation of ASIC1a drives RA synovial cell proliferation via the Wnt/β-catenin/c-Myc signaling pathway, an effect significantly attenuated by the ASIC1a inhibitor Psalmotoxin-1 (PcTx-1). In vivo studies corroborate that PcTx-1 mitigates synovial hyperplasia and cartilage degradation in adjuvant arthritis models [23]. In RA synovial tissue and fibroblast-like synovial cells (HFLS-RA), CDKN1A expression is significantly downregulated. Overexpression of CDKN1A induces G0/G1 cell cycle arrest, thereby inhibiting HFLS-RA proliferation and invasion, reducing pro-inflammatory cytokine levels (TNF-α and IL-6), and increasing anti-inflammatory cytokine expression (IL-10) [24]. Elevated miR-146a levels in RA tissues negatively regulate CDKN1A, while anti-miR-146a intervention effectively reduces HFLS-RA proliferation and invasion, decreases pro-inflammatory cytokine expression, and enhances anti-inflammatory cytokine levels [24]. Curcumin, another RA therapeutic candidate, has been shown to inhibit osteoclastogenesis in peripheral blood mononuclear cells by suppressing MAPK signaling pathways, including ERK1/2, p38, and JNK. This suppression inhibits the expression of RANK, c-Fos, and NFATc1, further highlighting its therapeutic potential [25]. Collectively, these findings suggest that the core components of Dunhuang Mofeng ointment exert multi-target therapeutic effects in RA by modulating key inflammatory and cellular signaling pathways. This multi-faceted approach underscores the formulation's potential as an effective intervention for RA.

MCL1, a pivotal anti-apoptotic molecule within the Bcl-2 family, plays an indispensable role in the survival of T and B lymphocytes as well as macrophages. In the synovial fluid of RA patients, CD14+ macrophages exhibit markedly elevated MCL1 expression. Inhibition of the PI3K/Akt-1 or STAT3 signaling pathways significantly reduces the proportion of CD14+ macrophages in synovial fluid, concomitantly downregulating MCL1 expression and inducing apoptosis in synovial macrophages. Furthermore, transfection of RA synovial macrophages with MCL1-specific siRNA induces apoptotic cell death, underscoring the critical role of MCL1 in macrophage survival [26]. Within the synovial tissue of RA patients, MCL1 expression is significantly upregulated in both the synovial membrane and subsynovial fibroblasts compared to control groups. This heightened expression correlates positively with inflammation severity and TNF-α levels. In vitro studies demonstrate that IL-1β stimulation induces a substantial increase in MCL1 mRNA and protein expression in synovial fibroblasts, a process essential for fibroblast survival. Adenovirus-mediated antisense MCL1 expression triggers fibroblast apoptosis via activation of pro-apoptotic molecules Bax, Bak, and Bim [27]. Elevated total STAT1 protein levels, alongside its activated

forms (tyrosine and serine phosphorylated), are consistently observed in RA synovium. STAT1 is predominantly localized in T and B lymphocytes undergoing focal inflammatory infiltration and in endosynovial fibroblast-like cells [28]. In vitro, fibroblast-like synoviocytes derived from RA patients exhibit constitutively higher STAT1 levels compared to those from osteoarthritis patients, with phosphorylation rapidly induced following IFN-β stimulation. Moreover, clinical studies have demonstrated that the efficacy of Baricitinib in RA patients correlates strongly with STAT1 phosphorylation in monocytes, suggesting that STAT1 phosphorylation may serve as an early biomarker for therapeutic response and a valuable reference point for treatment optimization [29]. CDK4/6, critical regulators of the cell cycle, also emerge as significant contributors to RA pathology. A double-blind, placebo-controlled Phase 1b clinical trial of the CDK4/6 inhibitor CTK-276 (≤175 mg) reported favorable tolerability in patients with active RA, with no significant safety concerns. At doses of ≥25 mg/day, TCK-276 demonstrated preliminary clinical efficacy, offering a promising avenue for further investigation into its therapeutic potential in active RA [30].

Although the classical TCMSP screening parameters (MW≤ 500, AlogP 1-3, and DL≥0.18) were originally developed for evaluating the DL of orally administered compounds, MW and lipophilicity are also key determinants influencing skin permeability. In general, compounds with MWs below 500 Da and moderate lipophilicity are considered more favorable for transdermal penetration. However, additional physicochemical factors, including the skin permeability coefficient, hydrogen bonding capacity, and polar surface area, may also influence the efficiency of transdermal delivery. Meanwhile, regardless of whether drugs are administered orally or topically, their absorption and distribution processes in vivo are affected by multiple physicochemical and biological factors. Therefore, DL parameters based on physicochemical properties may still provide certain reference value. In addition, the network pharmacology results in this study were further supported by mRNA expression analysis and animal experimental evidence, suggesting that the potential active components identified based on the above screening criteria are reliable within the context of this study. Therefore, the screening strategy adopted in this study primarily aims to identify potential bioactive compounds with reasonable physicochemical properties rather than to directly predict their transdermal pharmacokinetic characteristics. Regarding the limitations of this study, the validation of the key signaling pathways predicted by network pharmacology was mainly performed at the mRNA level, while the corresponding protein expression levels and phosphorylation status were not further examined. Due to factors such as post-transcriptional regulation, changes in mRNA expression do not necessarily fully reflect protein expression levels. Therefore, future studies are still required to further verify the related signaling pathways at the protein level using methods such as Western blot or other protein-based assays. On the other hand, the present study has already provided experimental validation of the predicted results at the animal level. Compared with studies that only perform validation at the cellular level, the in vivo validation conducted in this study enhances the reliability and biological relevance of the findings to a certain extent.

5 CONCLUSION

Through network pharmacological analysis and molecular docking studies, this investigation identified the core active constituents of Dunhuang Mofeng extract, namely quercetin, apigenin, luteolin, aloe-emodin, and emodin, with key molecular targets including CCND1, MYC, CDKN1A, FOS, MCL1, STAT1, and CDK4. In vitro pharmacodynamic assays further substantiated the significant therapeutic effects of Dunhuang Mofeng ointment in CIA rats. The underlying mechanism of action appears to involve the inhibition of pro-inflammatory cytokines such as TNF-α, IL-1β, and IL-6, while simultaneously promoting the release of the anti-inflammatory cytokine IL-10. These actions collectively contribute to the alleviation of foot and ankle joint swelling and pain, as well as the reduction of tissue edema in the rats. Additionally, the validation of molecular docking predictions was achieved by comparing the expression levels of STAT1, CDK4, CCND1, MCL1, FOS, CDKN1A, and MYC across experimental groups, confirming that the therapeutic effects of Dunhuang Mofeng ointment are likely mediated through the downregulation of these critical mRNA markers. This study provides a robust theoretical foundation for the continued investigation of Dunhuang Mofeng ointment as a potential treatment for RA. However, despite the successful achievement of the study objectives, there are inherent limitations in the experimental design, particularly concerning the selection of experimental endpoints and the need for further validation. Future research should focus on expanding the range of experimental indicators to facilitate a more comprehensive and in-depth elucidation of the precise molecular mechanisms underlying the observed therapeutic effects.

DECLARATIONS

Author contributions

HlZ conceived the initial idea of the study, collected and organized the relevant literature and data, performed data processing and preliminary analysis, prepared the figures and tables, and drafted the manuscript. JP assisted with data collection, literature screening, data curation, and manuscript formatting, and participated in revising the draft for important intellectual content. ZJS supervised the overall study, contributed to the study design and framework development, critically revised the manuscript for important intellectual content, and approved the final version for submission.

Funding

The authors declare that financial support was received for the research, authorship, and/or publication of this article. This

study was supported by the National Natural Science Foundation of China (81960877), the University Innovation Fund of Gansu Province (2021A-076), the Gansu Province Science and Technology Plan (Innovation Base and Talent Plan) (21JR7RA561), the Natural Science Foundation of Gansu Province (21JR1RA267), the Education Technology Innovation Project of Gansu Province (2022A-067), and the Open Project of the Key Laboratory of Dunhuang Medicine and Transformation, Ministry of Education (DHYX21-07, DHYX22-05, and DHYX21-01). Additional support was provided by the Gansu Province Joint Fund General Program (24JRRA878), the Gansu Provincial Science and Technology Program Project (24JRRA1020 and 25JRRA249), the Gansu Province Key Talent Program (2025RCXM006), the Teaching Research and Reform Program for Postgraduate Education at Gansu University of Traditional Chinese Medicine (YBXM-202406), and the Special Fund for Mentors of "Qihuang Talents" in the First-Level Discipline of Chinese Medicine (ZYXKBD-202415 and ZYXKSD-202415).

Data availability

The datasets used or analyzed during the current study are available from the corresponding author upon reasonable request.

Ethics approval and consent to participate

All animal experiments in this study were conducted in accordance with the relevant guidelines and regulations and were approved by the Animal Ethics Committee of Gansu University of Chinese Medicine (Approval Number: SY2023-966).

Consent for publication

Not applicable.

Competing interests

The authors declare that they have no competing interests.

Acknowledgements

Not applicable.

REFERENCES

[1] Finckh A, Gilbert BTP, Hodkinson B, Bae SC, Thomas R, Deane KD, et al. Global epidemiology of rheumatoid arthritis. Nat Rev Rheumatol. 2022 Oct;18(10):591-602. https://doi.org/10.1038/s41584-022-00827-y

[2] Alivernini S, Firestein GS, McInnes IB. The pathogenesis of rheumatoid arthritis. Immunity. 2022 Dec 13;55(12):2255-2270. https://doi.org/10.1016/j.immuni.2022.11.009

[3] Prasad P, Verma S, Surbhi, Ganguly NK, Chaturvedi VP, Mittal SA. Rheumatoid arthritis: Advances in treatment strategies. Mol Cell Biochem. 2022 Jan;478(1):69-88. https://doi.org/10.1007/s11010-022-04492-3

[4] Huang J, Fu X, Chen X, Li Z, Huang Y, Liang C. Promising therapeutic targets for treatment of rheumatoid arthritis. Front Immunol. 2021 Jul 9;12:686155. https://doi.org/10.3389/fimmu.2021.686155

[5] Aihaiti Y, Song Cai Y, Tuerhong X, Ni Yang Y, Ma Y, Shi Zheng H, et al. Therapeutic effects of naringin in rheumatoid arthritis: Network pharmacology and experimental validation. Front Pharmacol. 2021 May 14;12:672054. https://doi.org/10.3389/fphar.2021.672054

[6] Mysler E, Caubet M, Lizárraga A. Current and emerging dmards for the treatment of rheumatoid arthritis. Open Access Rheumatol. 2021 Jun 1;13:139-152. https://doi.org/10.2147/OARRR.S282627

[7] Hu Y, Zhu W, Wang X, Yu Y, Shi K, Meng Q. Experiences of chinese rheumatoid arthritis patients who chose western medicine, traditional chinese medicine, and a combination of treatments: A study based on interviews and thematic analysis. Patient Prefer Adherence. 2024 Jul 4;18:1423-1433. https://doi.org/10.2147/PPA.S463218

[8] Sharma YK, Philip VM, Sharma S. Prospective, open-label, randomized, parallel group, comparative clinical study of two topical formulations of diclofenac diethylamine in the treatment of acute painful musculoskeletal conditions. J Mar Med Soc. 2020;22:35-39. https://doi.org/10.4103/jmms.jmms_58_19

[9] Wiffen PJ, Xia J. Systematic review of topical diclofenac for the treatment of acute and chronic musculoskeletal pain. Curr Med Res Opin. 2020 Apr;36(4):637-650. https://doi.org/10.1080/03007995.2020.1716703

[10] Taylor RS, Fotopoulos G, Maibach HI. Safety profile of topical diclofenac: A meta-analysis of blinded, randomized, controlled trials in musculoskeletal conditions. Curr Med Res Opin. 2011 Mar;27(3):605-622. https://doi.org/10.1185/03007995.2010.550606

[11] Tang M, Zeng Y, Peng W, Xie X, Yang Y, Ji B, et al. Pharmacological aspects of natural quercetin in rheumatoid arthritis. Drug Des Devel Ther. 2022 Jun 29;16:2043-2053. https://doi.org/10.2147/DDDT.S364759

[12] Yuan K, Zhu Q, Lu Q, Jiang H, Zhu M, Li X, et al. Quercetin alleviates rheumatoid arthritis by inhibiting neutrophil inflammatory activities. J Nutr Biochem. 2020 Oct;84:108454. https://doi.org/10.1016/j.jnutbio.2020.108454

[13] Javadi F, Ahmadzadeh A, Eghtesadi S, Aryaeian N, Zabihiyeganeh M, Rahimi Foroushani A, et al. The effect of quercetin on inflammatory factors and clinical symptoms in women with rheumatoid arthritis: A double-blind, randomized controlled trial. J Am Coll Nutr. 2017 Jan;36(1):15-19. https://doi.org/10.1080/07315724.2016.1140093

[14] Kim HR, Kim BM, Won JY, Lee KA, Ko HM, Kang YS, et al. Quercetin, a plant polyphenol, has potential for the prevention of bone destruction in rheumatoid arthritis. J Med Food. 2019 Feb;22(2):152-161. https://doi.org/10.1089/jmf.2018.4259

[15] Sun QW, Jiang SM, Yang K, Zheng J, Zhang L, Xu W. Apigenin enhances the cytotoxic effects of tumor necrosis factor-related apoptosis-inducing ligand in human rheumatoid arthritis fibroblast-like synoviocytes. Mol Biol Rep. 2012 May;39(5):5529-5535. https://doi.org/10.1007/s11033-011-1356-3

[16] Shin GC, Kim C, Lee J, Cho WS, Lee SG, Jeong M, et al. Apigenin-induced apoptosis is mediated by reactive oxygen species and activation of ERK1/2 in rheumatoid fibroblast-like synoviocytes. Chem Biol Interact. 2009 Nov 10;182(1):29-36. https://doi.org/10.1016/j.cbi.2009.07.016

[17] Shi F, Zhou D, Ji Z, Xu Z, Yang H. Anti-arthritic activity of luteolin in freund's complete adjuvant-induced arthritis in rats by suppressing P2X4 pathway. Chem Biol Interact. 2015 Jan 25;226:82-87. https://doi.org/10.1016/j.cbi.2014.10.031

[18] Hu B, Zhang H, Meng X, Wang F, Wang P. Aloe-emodin from rhubarb (Rheum rhabarbarum) inhibits lipopolysaccharide-induced inflammatory responses in RAW264.7 macrophages. J Ethnopharmacol. 2014 May 14;153(3):846-853. https://doi.org/10.1016/j.jep.2014.03.059

[19] Cheng L, Chen J, Rong X. Mechanism of emodin in the treatment of rheumatoid arthritis. Evid Based Complement Alternat Med. 2022 Oct 3;2022:9482570. https://doi.org/10.1155/2022/9482570

[20] Zhu M, Yuan K, Lu Q, Zhu Q, Zhang S, Li X, et al. Emodin ameliorates rheumatoid arthritis by promoting neutrophil apoptosis and inhibiting neutrophil extracellular trap formation. Mol Immunol. 2019 Aug;112:188-197. https://doi.org/10.1016/j.molimm.2019.05.010

[21] Tao SS, Fang X, Xu L, Zhang RD, Luo QQ, Tang J, et al. Association of gene polymorphisms and the decreased expression of long non-coding RNA LOC553103 with rheumatoid arthritis. Postgrad Med J. 2024 Apr 24:qgae055. https://doi.org/10.1093/postmj/qgae055

[22] Lee J, Jeong H, Park EJ, Hwang J, Huang B, Bae E, et al. CIP2A facilitates apoptotic resistance of fibroblast-like synoviocytes in rheumatoid arthritis independent of c-Myc expression. Rheumatol Int. 2013 Sep;33(9):2241-2248. https://doi.org/10.1007/s00296-013-2711-6

[23] Xu Y, Lu Z, Ling Y, Hou R, Tao JJ, Deng G, et al. Acid sensor ASIC1a induces synovial fibroblast proliferation via Wnt/β-catenin/c-Myc pathway in rheumatoid arthritis. Int Immunopharmacol. 2022 Dec;113(Pt A):109328. https://doi.org/10.1016/j.intimp.2022.109328

[24] Gang X, Xu H, Si L, Zhu X, Yu T, Jiang ZD, et al. Treatment effect of CDKN1A on rheumatoid arthritis by mediating proliferation and invasion of fibroblast-like synoviocytes cells. Clin Exp Immunol. 2018 Nov;194(2):220-230. https://doi.org/10.1111/cei.13161

[25] Shang W, Zhao LJ, Dong XL, Zhao ZM, Li J, Zhang B, et al. Curcumin inhibits osteoclastogenic potential in PBMCs from rheumatoid arthritis patients via the suppression of MAPK/RANK/c-Fos/NFATc1 signaling pathways. Mol Med Rep. 2016 Oct;14(4):3620-3626. https://doi.org/10.3892/mmr.2016.5674

[26] Liu H, Huang Q, Shi B, Eksarko P, Temkin V, Pope RM. Regulation of Mcl-1 expression in rheumatoid arthritis synovial macrophages. Arthritis Rheum. 2006 Oct;54(10):3174-3181. https://doi.org/10.1002/art.22132

[27] Liu H, Eksarko P, Temkin V, Haines GK, Perlman HR, Koch AE, et al. Mcl-1 is essential for the survival of synovial fibroblasts in rheumatoid arthritis. J Immunol. 2005 Dec 15;175(12):8337-8345. https://doi.org/10.4049/jimmunol.175.12.8337

[28] Kasperkovitz PV, Verbeet NL, Smeets TJ, van Rietschoten JG, Kraan MC, van der Pouw Kraan TC, et al. Activation of the stat1 pathway in rheumatoid arthritis. Ann Rheum Dis. 2004 Mar;63(3):233-239. https://doi.org/10.1136/ard.2003.013276

[29] Tucci G, Garufi C, Pacella I, Zagaglioni M, Pinzon Grimaldos A, Ceccarelli F, et al. Baricitinib therapy response in rheumatoid arthritis patients associates to stat1 phosphorylation in monocytes. Front Immunol. 2022 Jul 25;13:932240. https://doi.org/10.3389/fimmu.2022.932240

[30] Tasaki D, Tsuruda K, Sun S, Tsumura Y, Asano S, Suzuki Y, et al. A double-blind, placebo-controlled, randomized multiple dose phase 1b trial of a CDK4/6 inhibitor, TCK-276, in patients with active rheumatoid arthritis. Rheumatology (Oxford). 2025 Mar 1;64(3):1036-1044. https://doi.org/10.1093/rheumatology/keae357